

DOE/PC/93217--T4

# Superior Catalysts for Selective Catalytic Reduction of Nitric Oxide

## Annual Technical Report

September 30, 1993 - September 29, 1994

### Submitted to:

Dr. Michael J. Baird

U.S. Department of Energy  
Pittsburgh Energy Technology Center

Under Contract DE-FG22-93PC93217

by

J. P. Chen, M. C. Hausladen and R. T. Yang

Department of Chemical Engineering  
State University of New York at Buffalo  
Buffalo, NY 14221

### **DISCLAIMER**

This report was prepared as an account of work sponsored by an agency of the United States Government. Neither the United States Government nor any agency thereof, nor any of their employees, makes any warranty, express or implied, or assumes any legal liability or responsibility for the accuracy, completeness, or usefulness of any information, apparatus, product, or process disclosed, or represents that its use would not infringe privately owned rights. Reference herein to any specific commercial product, process, or service by trade name, trademark, manufacturer, or otherwise does not necessarily constitute or imply its endorsement, recommendation, or favoring by the United States Government or any agency thereof. The views and opinions of authors expressed herein do not necessarily state or reflect those of the United States Government or any agency thereof.

**MASTER**

ACQUISITION & ASSISTANCE DIV.

55 JAN 23 AM 3:04

RECEIVED  
USDOE/PETC

DISTRIBUTION OF THIS DOCUMENT IS UNLIMITED

*Z n/mg*

## **DISCLAIMER**

**Portions of this document may be illegible in electronic image products. Images are produced from the best available original document.**

**ABSTRACT**

A delaminated Fe<sub>2</sub>O<sub>3</sub>-pillared clay catalyst was prepared for the selective catalytic reduction (SCR) of NO by NH<sub>3</sub> at above 300°C. The delaminated pillared clay was characterized by ICP-AES (Inductively Coupled Plasma - Atomic Emission Spectroscopy) chemical analysis, XRD (X-ray diffraction) structure and line broadening analyses, micropore size probing, and Mössbauer analysis. These analyses showed that the catalyst contained fragmented Fe<sub>2</sub>O<sub>3</sub>-pillared clay forming "house-of-cards" structure with dispersed Fe<sub>2</sub>O<sub>3</sub> particles approximately 170 Å in size. The SCR activity of the delaminated pillared clay was higher than the commercial-type V<sub>2</sub>O<sub>5</sub> + WO<sub>3</sub>/TiO<sub>2</sub> catalyst, and also higher than the undelaminated pillared clay and supported Fe<sub>2</sub>O<sub>3</sub> catalysts, under conditions without SO<sub>2</sub>. Infrared measurements of adsorbed NH<sub>3</sub> showed strong Brønsted acidity which was caused possibly by interactions between Fe<sub>2</sub>O<sub>3</sub> and clay.

## INTRODUCTION

Selective catalytic reduction (SCR) of nitrogen oxides with ammonia is of increasing industrial importance. A comprehensive review of the subject is available (1). The commercial catalysts are  $V_2O_5$  with mixed  $WO_3$  and/or  $MoO_3$  supported on  $TiO_2$ . A direct correlation between the SCR activity and the Brønsted acidity of  $V_2O_5$  has been observed (2-5), and the Brønsted acid sites are thought to be the active sites. Besides  $V_2O_5$ , a large number of catalysts have activities for the SCR reaction, some of which have also been reviewed. First results of SCR activities on pillared clays and potential advantages of using pillared clays have been reported by Yang et al. (6).

Pillared interlayered clays (PILC), or pillared clays, are two-dimensional zeolite-like materials prepared by exchanging the charge-compensating cations between the clay layers with large inorganic hydroxycations, which are polymeric or oligomeric hydroxy metal cations formed by hydrolysis of metal oxides or salts. Upon heating, the metal hydroxycations undergo dehydration and dehydroxylation, forming stable metal oxide clusters which act as pillars keeping the silicate layers separated, creating interlayer space (gallery) of molecular dimensions. Much interest and research have been directed to metal oxide PILC since their first successful syntheses in late 1970s (7-11). Comprehensive reviews of the voluminous literature on the subject are available (12-14). In principle, any metal oxide or salt that forms polynuclear species upon hydrolysis (15) can be inserted as pillars, and all layered clays of the abundant phyllosilicate family as well as other layered clays can be used as the hosts (References cited in 13, and 16-18). Because of its large pores and hydrothermal stability (to  $700^\circ\text{C}$ ), the main early interest in PILC was in the possibility of replacing zeolite as the catalyst for fluid catalytic cracking (11,19). However, this possibility has been hindered due to excessive carbon deposition and limited hydrothermal stability. An additional difficulty was that the pore size could be considerably smaller than the interlayer spacing calculated from XRD. For Zr-PILC, the interpillar spacings in the range of 4-8 Å were the limiting pore sizes although XRD results showed an interlayer spacing of 14.6 Å (20,21). Besides FCC, PILCs have been studied for

catalyzing alcohol dehydration (22,23), alkylation and other acid catalyzed reactions (23,24,25). A pillared titanium phosphate was used as the support, for  $V_2O_5$  for the SCR reaction (26).

Despite many studies on the acid sites on PILCs, the nature and properties of these sites are not well understood (11,14,27,28). The acidity and acid site types (Brønsted or Lewis) depend on the exchanged cations, preparation method and the starting clay. Both Lewis and Brønsted acid sites exist on pillared clays, with a larger proportion being Lewis acid sites. Our discussion will be focused on the Brønsted acidity because of its importance to the SCR reaction. Two sources for Brønsted acidity have been discussed in the literature. One derives from the structural hydroxyl groups in the clay layer (27). The most likely proton site for some smectites (e.g., montmorillonite) is located at the A1(VI)-O-Mg linkage, where A1(VI) is the octahedrally coordinated A1, and Mg is one that has substituted an A1 in the octahedral layer. For other clays, e.g., beidellite and saponite, the proton sites are located at the Si-O-AlOH- groups resulting from isomorphous substitution of Si by Al in the tetrahedral layer. Another likely source for protons derives from the cationic oligomers which upon heating decompose into metal oxide pillars and liberate protons. It has been reported from many studies that both Lewis and Brønsted acidities decrease with temperature of calcination (14,27). The disappearance of Brønsted acidity is attributed to the migration of protons from the interlayer surfaces to the octahedral layer within the clay layer where they neutralize the negative charge at the substitution atoms (such as Mg) (29). However, of particular significance to our study on the SCR reaction is the fact that upon exposure to  $NH_3$  the migration can be reversed so the proton is again available on the surface (29,30). Although the total acidity appears to vary with the kind of metal oxide inserted as pillars (27), Brønsted acidity appears to be insensitive to the kind of metal oxide pillars so far used (35).

A potential major advantage of pillared clays for SCR application is the resistance to poisoning. The chemistry of poisoning of the Brønsted acid sites is reasonably understood (4). However, a significant contributor to catalyst poisoning is apparently the deposition of  $As_2O_3$  and other vapor species within the pore structure of the vanadia catalyst. This problem can be

alleviated by a new catalyst design by Hegedus and coworkers (31), which consists of a bimodal pore size distribution in the  $V_2O_5/TiO_2-SiO_2$  catalyst: one group of pores are of the order of microns (macropores) and the other group are of the order of angstroms (micropores). The poisonous vapor species in the flue gas such as  $As_2O_3$  deposit on the walls of the macropores due to their low diffusivities. Since the macropores serve as feeder pores to the micropores, they provide the function as filters of poisons. The pore structure of any catalysts made of pillared clays would be unavoidably bimodal. The commercially available clays such as montmorillonite are of particle sizes of microns or fraction of a micron. A pelletized (or washcoat) PILC catalyst will contain feeder (or poison filter) pores in the interparticle spaces, whereas the intraparticle micropores contain the active catalyst surface for the SCR reaction.

Another class of pillared clays, termed "delaminated clays," was first synthesized by Pinnavaia et al. (32). These PILC's are prepared with the same procedures except that freeze-drying is used, instead of air-drying, after the ion exchange step. Alumina and chromia clays have been made in this manner. These clays do not exhibit long-range layer stacking as evidenced by the absence of the 001 X-ray reflections. However, it is believed that short-range stacking with pillared structure still exists, and the overall structure is described as "house-of-cards." These clays contain both micropores and macropores (33). The introduction of macropores can significantly increase the diffusion rates, hence the overall activities are increased (as well as altering product distribution in hydrocarbon cracking (19,32-35)).

## **EXPERIMENTAL**

**Experimental Apparatus and Rate Measurement.** The reactor system for the SCR reaction was the same as described elsewhere (6). The reactor consisted of a quartz tube. The heating element was a coiled Nichrome wire. The reactor temperature was controlled by an Omega CN-2010 programmable temperature controller. The catalyst, typically 0.4 g, was supported on a fritted support.

Two sets of flow meters were employed for blending a synthetic flue gas. Rotameters were used to control flows with high flow rates (i.e.,  $N_2$ ,  $NH_3 + N_2$  and  $NO + N_2$ ). Mass flow

meters were used for gases with low flow rates ( $\text{SO}_2$  and  $\text{O}_2$ ). The pre-mixed gases (0.8% NO in  $\text{N}_2$  and 0.8%  $\text{NH}_3$  in  $\text{N}_2$ ) were supplied by Linde Division. Water vapor was generated by passing nitrogen through a heated gas-wash bottle containing distilled water. To prevent the deposition of ammonium sulfate, the tubings were heated by heating tapes. NO concentration was continuously monitored by a chemiluminescent NO/ $\text{NO}_x$  analyzer (Thermo Electron Corporation, Model 10). To avoid any analytical error caused by oxidation of ammonia in the converter of the NO/ $\text{NO}_x$  analyzer, an ammonia trap (phosphoric acid solution) was installed before the sample inlet.

The absence of intrapellet mass transfer resistance under the experimental conditions has been discussed previously (4), achieved by minimizing the pellet size. The size range for the catalyst was 100-150 US mesh. However, the intracrystalline diffusion resistance was clearly present.

**Syntheses of Pillared Clays (PILC).** The general method for PILC synthesis is given first, which will be followed by details for the syntheses of the specific pillared clays used in this study. The first step in PILC synthesis is preparation and aging of the pillaring solution to form oligomers. The pillaring agent undergoes hydrolysis, polymerization and complexation with anions in the solution (13,15). The hydrolysis conditions are important to the formation of PILC: temperature, pH and aging time.

**Synthesis of Delaminated Pillared Clay.** The clay suspension solution was prepared by dispersing 10 grams of bentonite (Fisher Scientific, purified grade) in 1 liter distilled water. Our chemical analysis showed that the bentonite from Fisher was mostly  $\text{Na}^+$  montmorillonite. The pillaring agent was prepared by hydrolysis of 3 liters of 0.2 M  $\text{Fe}(\text{NO}_3)_3$ , and anhydrous sodium carbonate was added to the vigorously stirred  $\text{Fe}(\text{NO}_3)_3$  solution to adjust the pH value of the solution.  $\text{CO}_2$  evolution occurred during hydrolysis. The resulting solution was aged for 24 hours at room temperature prior to use. The ratio of base to iron was equal to 2, i.e.,  $\text{OH}^-/\text{Fe} = 2$ , and the final pH value of the solution was 1.8. The aqueous clay suspension was dropwise added to the polyoxoiron cation solution through a funnel. The cation exchange capacity of the

bentonite was 103 meq/100g. The ratio of Fe/clay was approximately 60 (mmole of Fe)/(m.e.q. of clay). The pillaring/delaminating (ion-exchange) reaction took place at room temperature. It was found that the nature of the pillared clay product depended on the reaction condition. Pillared clay resulted from short (e.g., below 3 hrs.) reaction times at near ambient temperature whereas delaminated pillared clay formed after long reaction times (e.g., over 12 hrs.) and at higher temperatures (40-50°C). The delamination could be caused by chemical interactions between the pillaring agent and the clay resulting in the breakdown of the clay texture. The delamination process is, however, not understood and is under further study. Both Fe<sub>2</sub>O<sub>3</sub>-PILC and delaminated Fe<sub>2</sub>O<sub>3</sub>-PILC were prepared and were subsequently subjected to SCR activity tests. After the reaction, the suspension solution was kept still to separate the top portion of the clear solution. The pillared/delaminated clay was separated by vacuum filtration of the suspension solution. The collected solid sample was redispersed and washed in distilled water. The final sample was collected after repeatedly dispersion/washing/filtration for three times. The collected solid samples were first dried at 120°C for 24 hours, then crushed and sieved to collect the desired fractions. The samples were further heated to 400°C at a rate of 2°C/min. in a tubular reactor and were kept at the temperature for a period of at least 12 hours. After these pretreatments, the samples were ready for further experiments.

**Chemical Composition Analysis.** The chemical composition of the delaminated pillared clay was analyzed by inductively coupled plasma atomic emission spectrometer (Thermo Jarrel Ash 61 ICAP). A fusion-dissolution method was used for sample preparation. The clay sample (0.1 gram) was fused with a mixture (0.6 gram total) of lithium metaborate and lithium tetraborate (at a weight ratio of 1:2) in a graphite crucible at 1000°C for about one hour. After slowly cooling to room temperature, the fluxed bead was dissolved in 250 ml hot 2% HNO<sub>3</sub> solution. When the fluxed bead dissolved completely, the solution was filtered to remove graphite fiber impurity that came from the crucible. The bentonite sample was analyzed by the same procedure.

**In situ Infrared Spectra.** IR spectra were measured with a Nicolet Impact 400 FT-IR spectrometer. The samples were pressed into self-supporting disks. The typical weight of the prepared disks was 60-70 mg, which was equivalent to 12-14 mg/cm<sup>2</sup>. The *in situ* IR spectra of NH<sub>3</sub> adsorbed on pillared/delaminated clays were recorded by using an IR cell that allowed the sample to be treated at high temperatures under vacuum or in different gases. The samples were pretreated at 300°C in vacuo for 2 hours prior to adsorption.

**X-Ray Diffraction Characterization.** X-ray diffraction patterns were obtained using powder samples in a Stoe transmission powder diffractometer with CuK $\alpha$  radiation. Normally, the data were collected in 2 minutes. For samples with weak signals or being amorphous, the data collection time was extended to at least 6 minutes.

XRD was also used to determine the Fe<sub>2</sub>O<sub>3</sub> particle size. The particle size measurement was based on X-ray line broadening using a method described by Klug and Alexander (35). Silicon was used as a standard for calibration of half-height line width.

**Mössbauer Spectra.** Transmission Mössbauer spectra were measured using a constant acceleration mode Mössbauer spectrometer with <sup>57</sup>Co source at room temperature. The catalyst pellets were ground into a powder and was dispersed and mounted on scotch tape to provide a sample diameter of 25 mm. Spectra are reported relative to iron foil.

**BET Surface Area and Molecular Probing for Pore Sizes.** BET surface areas were measured by adsorption of nitrogen at 77K using a Quantasorb sorption system.

Thermogravimetric analysis (TGA) was employed to measure the weight gains, by sorption of molecules with known dimensions. Pore volumes for different pore dimensions were measured in this manner.

## **RESULTS AND DISCUSSION**

### **Chemical Compositions and BET Areas**

Inductive coupled argon plasma spectrometric method (ICP) was used for chemical composition analyses. Because of the existence of sodium in the clay samples, sample preparation was done by fusion with lithium borate followed by dissolution for ICP analyses

(37). The ICP results are shown in Table 1. The water contents in Table 1 were obtained separately by thermo-gravimetric analysis (TGA) by heating in helium to 400°C.

Table 1 shows that after ion exchange/pillaring reaction, the contents of the cations,  $\text{Na}^+$ ,  $\text{K}^+$ ,  $\text{Ca}^{++}$  and  $\text{Mg}^{++}$ , decreased. However, the most significant change in the synthesized samples was the iron oxide content, which increased from 3.66% to up to 30.61%. The iron oxide pillared clay contained about 10% iron oxide. The larger amount of iron oxide in delaminated/pillared clay was the result of the interactions between the clay and the pillaring solution at higher temperatures and for a longer time. These surface iron oxide particles were further analyzed by XRD and Mössbauer measurements.

BET surface area measurements showed that the BET area of the pillared/delaminated clay increased from 24 to 155  $\text{m}^2/\text{g}$  whereas that of the  $\text{Fe}_2\text{O}_3$ -PILC increased from 24 to 212  $\text{m}^2/\text{g}$ . These BET surface areas are consistent with the range of typical values for  $\text{Fe}_2\text{O}_3$ -PILC of 125-324  $\text{m}^2/\text{g}$  (75). The low value of the pillared/delaminated clay could be caused by the supported iron oxide particles blocking some of the pores.

### Structural Analysis by X-Ray Diffraction

X-ray diffraction (powder) patterns of the starting clay (bentonite) are shown in Figure 1. Pattern A was recorded without pre-treatment. Pattern B was recorded after the sample was calcined at 300°C for two hours. The decrease of  $d_{001}$  spacing from 12.1 to 9.85 Å was due to dehydration of the interlayer hydrates.

XRD patterns of smectite clays generally show basal  $001$  reflection and two dimensional diffraction  $hk$  only (38,39). Other  $hkl$  reflections are usually not observed. The random or unoriented clay sample only show a strong  $001$  diffraction; the  $hk$  diffractions are also strong but diffusive (Figure 1). The characteristics of the  $hk$  diffractions is that the peak terminates steeply at the low-angle side but falls off gradually at the high-angle side. The  $hk$  reflections are characteristic of the type of the clay mineral, whereas the  $(001)$  basal reflection is characteristic of the conditions, i.e., interlayer water, cations, etc.

**Table 1. Chemical Compositions (% by wt.) and BET Surface Areas  
of Clay and Pillared Clays**

	<b>Montmorillonite</b>	<b>Delaminated Fe<sub>2</sub>O<sub>3</sub>-PILC</b>	<b>Fe<sub>2</sub>O<sub>3</sub>-PILC</b>
<b>SiO<sub>2</sub></b>	60.32	44.36	59.19
<b>Al<sub>2</sub>O<sub>3</sub></b>	19.14	13.93	19.63
<b>Fe<sub>2</sub>O<sub>3</sub></b>	3.66	30.61	9.55
<b>TiO<sub>2</sub></b>	0.16	0.15	0.18
<b>CaO</b>	1.41	0.55	0.47
<b>MgO</b>	2.35	1.56	2.06
<b>Na<sub>2</sub>O</b>	2.88	0.59	0.65
<b>K<sub>2</sub>O</b>	0.51	0.33	0.34
<b>H<sub>2</sub>O</b>	8.50	3.54	3.06
<b>Total</b>	98.93	95.61	95.13
<b>BET Surface Area (m<sup>2</sup>/g)</b>	24	155	212

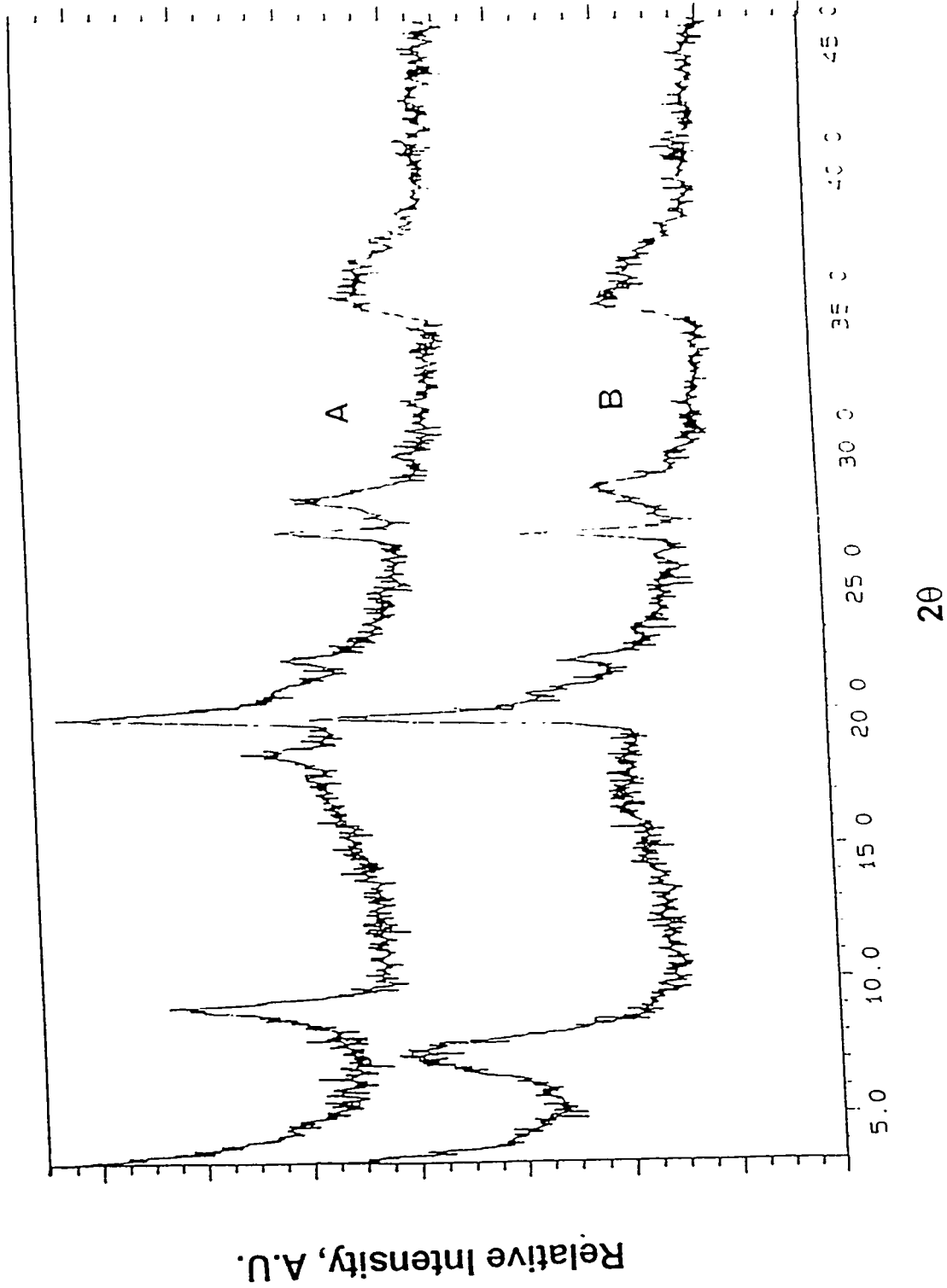


Figure 1 XRD patterns of bentonite (CuK $\alpha$  source). A: No pretreatment; B: Calcined at 300°C for 2 hours.

Other major peaks in Fig. 1 are assigned as follows (40,41). The peaks at  $2\theta$  of  $19.6^\circ$  ( $d = 4.49 \text{ \AA}$ ) and  $34.9^\circ$  ( $d = 2.57 \text{ \AA}$ ) are assigned to the two dimensional diffraction,  $hk$ , reflections. These non-basal  $hk$  two-dimensional reflections arise from the diffraction of the random stacking of layers. Each observed  $hk$  reflection is the summation of several  $hk$  index pairs. The diffraction at  $19.6^\circ$  ( $d = 4.49 \text{ \AA}$ ) is the summation of  $hk$  indices of (02) and (11), and the diffraction at  $34.9^\circ$  ( $d = 2.57 \text{ \AA}$ ) is the summation of  $hk$  indices of (13) and (20). The two-dimensional  $hk$  reflections are strongest in unoriented crystals. The peak at  $2\theta = 26.5^\circ$  ( $d = 3.36 \text{ \AA}$ ) is the diffraction of (101) from quartz impurity.

The XRD patterns of the synthesized clay catalysts are shown in Fig. 2. In the  $\text{Fe}_2\text{O}_3$ -pillared clay sample, the  $d_{001}$  spacing was  $26.4 \text{ \AA}$ , and the two-dimensional  $hk$  reflections remained. For the delaminated sample, no reflections were observed in the  $2\theta$  range  $3\text{-}45^\circ$ . The disappearance of the regular basal spacing of clay and the distinct lines corresponding to larger interlayer spacing (i.e.,  $2\theta < 5^\circ$ ) was also observed by Burch and Warburton (42) in their preparation of  $\text{Fe}_2\text{O}_3$  pillared clay. Pillared clays that exhibit no (001) reflection have been referred to as "delaminated clay" (14,32) in the literature.

The XRD analysis showed that the delaminated sample not only lost its (001) diffraction, but also the two-dimensional diffraction peaks at  $d$ -spacings equal to  $4.49 \text{ \AA}$  and  $2.57 \text{ \AA}$ , i.e., the clay lost its two dimensional characteristic diffractions. As discussed by Ocelli et al. (19), the delaminated clay does not preclude the possibility of short range ordering in the interlayer direction. Also the absence of the two dimensional reflections does not mean that there was no short range two dimensional structure in the clay. Rather, the large two dimensional structure could have been fragmented into small pieces giving a semi-amorphous form. These small pieces would be the basic units in the structure referred to as "house-of-cards," which have shown to be superior over the normal pillared clays in many aspects (19,32,33,43,44).

#### **Micropore Size Distribution by Molecular Probing**

The existence of micropores and the micropore size distribution in the delaminated clay sample were further studied by sorption of probe molecules at subcritical temperatures. Under

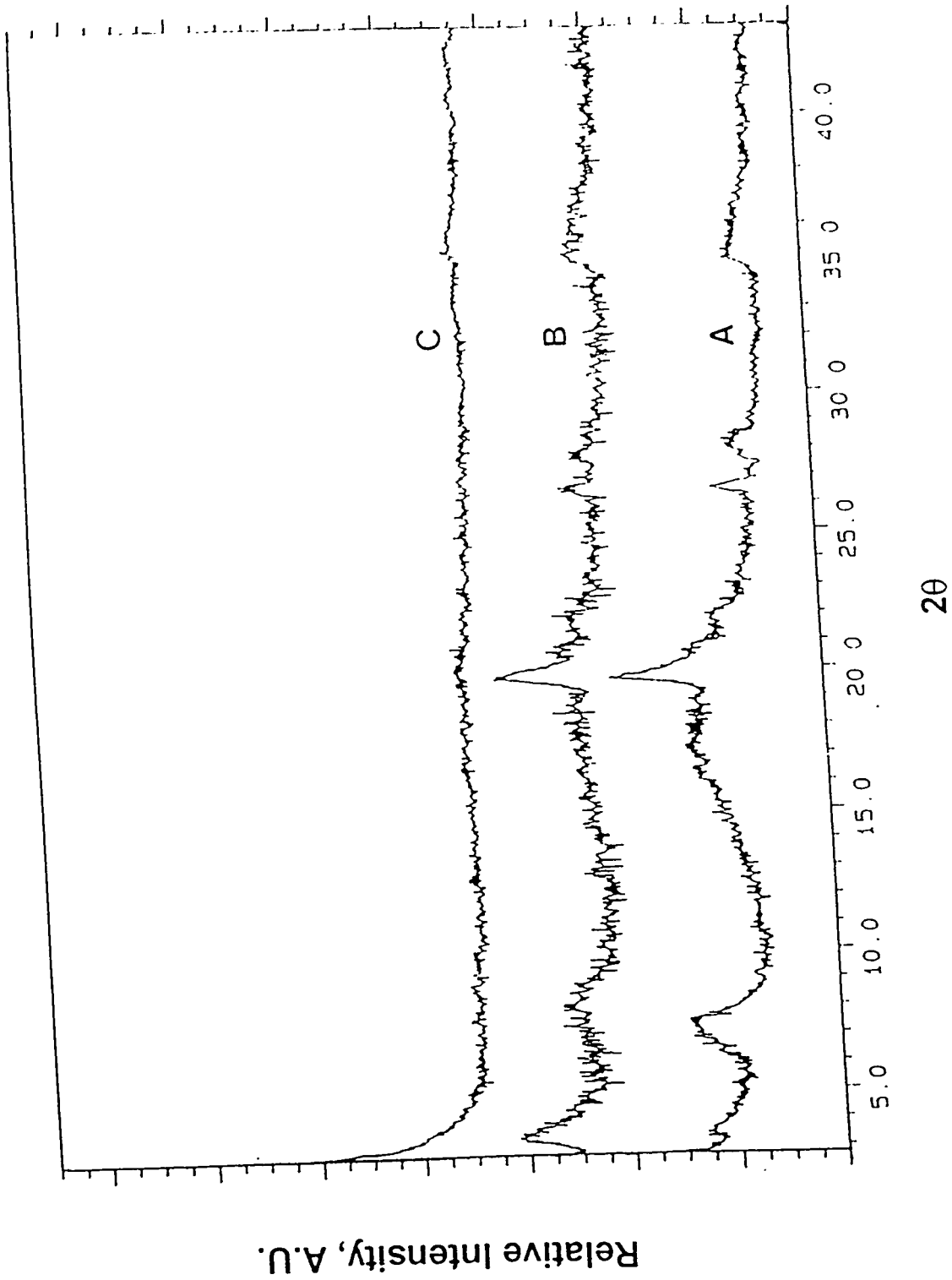


Figure 2 XRD patterns ( $\text{CuK}\alpha$  source) of bentonite (A);  $\text{Fe}_2\text{O}_3$ -pillared clay (B); and delaminated pillared clay (C).

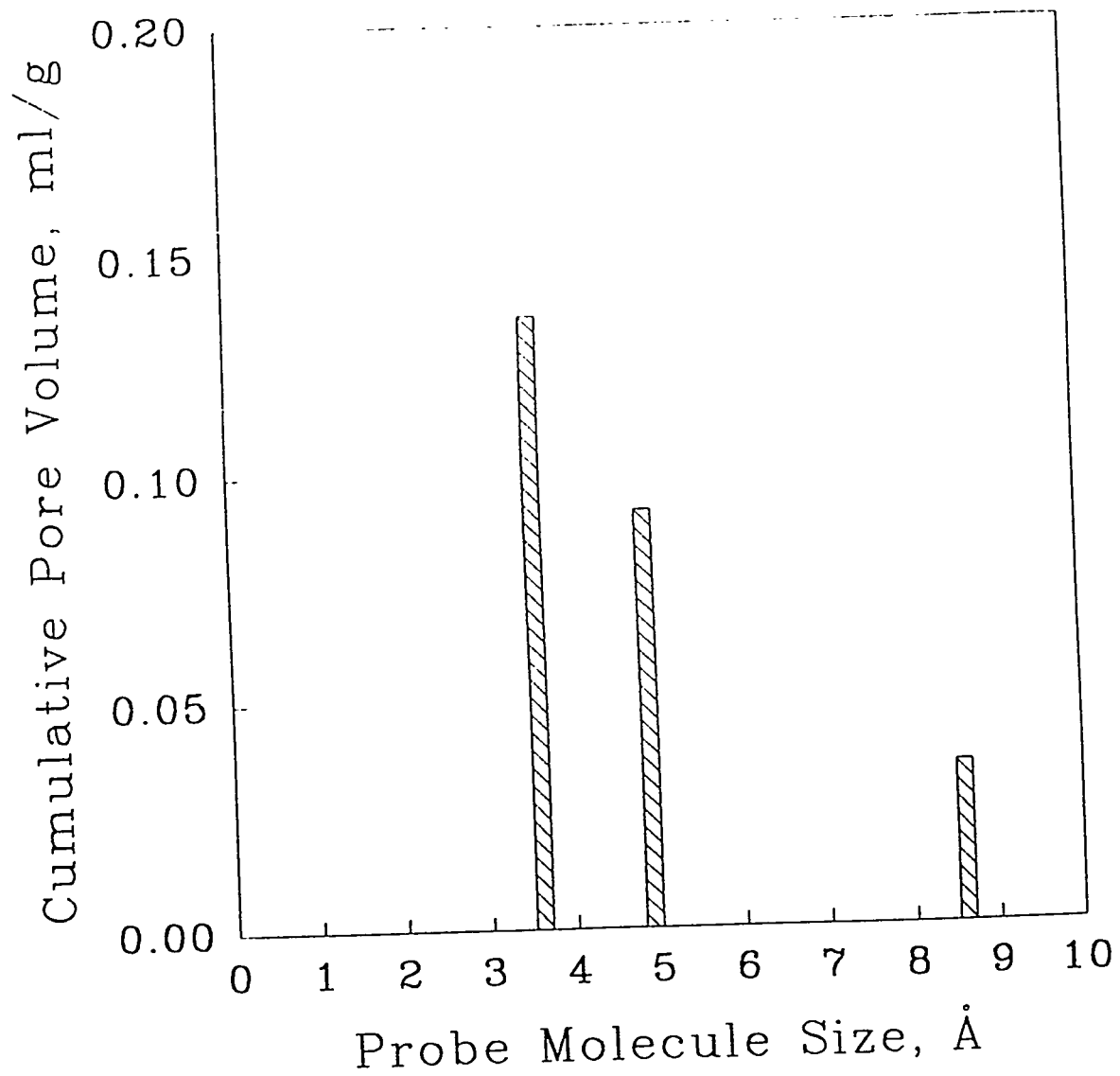


Figure 3 Cumulative micropore volume as a function of pore dimension measured by micropore filling with probe molecules ( $\text{N}_2 = 3.6 \text{ \AA}$ , n-hexane =  $4.9 \text{ \AA}$  and 1,3,5-trimethyl benzene =  $8.6 \text{ \AA}$ ).

subcritical conditions, micropore filling takes place and the micropore volumes can be calculated (21,45).

Three probe molecules were used, with their kinetic diameters given below: N<sub>2</sub> (3.6 Å), n-hexane (4.9 Å) and 1,3,5 trimethyl benzene (8.6 Å). The cumulative pore volumes were calculated from the equilibrium sorption amount assuming the adsorbate as liquid. The equilibrium sorption amounts of n-hexane and trimethyl benzene were measured at room temperature by TGA (Thermogravimetric Analysis). The N<sub>2</sub> sorption was measured at 77K with the Quantasorb Analyzer. The results are shown in Fig. 3. For the N<sub>2</sub> sorption, the  $\alpha_s$  method was used to obtain the micropore volume (45). From the data shown in Fig. 3, it is seen that a significant amount of micropores with dimensions smaller than 9 Å existed in the delaminated sample. For the Fe<sub>2</sub>O<sub>3</sub>-pillared clay (21), the cumulative pore volume by N<sub>2</sub> sorption was 0.19 cm<sup>3</sup>/g, compared to 0.13 cm<sup>3</sup>/g for the delaminated clay. From this result, it is clear that the delaminated sample contained pillared clay fragments, thus it should be properly referred to as delaminated pillared clay.

### **Fe<sub>2</sub>O<sub>3</sub> Particle Size by XRD Line Broadening**

The chemical composition analysis indicated that there were Fe<sub>2</sub>O<sub>3</sub> particles in addition to the fragmented Fe<sub>2</sub>O<sub>3</sub>-pillared clay. The Fe<sub>2</sub>O<sub>3</sub> particle size was analyzed by XRD and Mössbauer.

As discussed, the X-ray diffraction patterns for the clay structure disappeared. However, the weak and broadened peaks at 2 $\theta$  of 33.36° (d = 2.686 Å) and 35.79° (d = 2.510 Å) became discernible by extending the data collection time to 400 seconds, as shown in Fig. 4. These two peaks were reflections by the (104) and (110) faces, respectively, of hematite (46).

From the line broadening, the particle size can be calculated with the following formula (36):

$$L = K\lambda / \beta \cos\theta$$

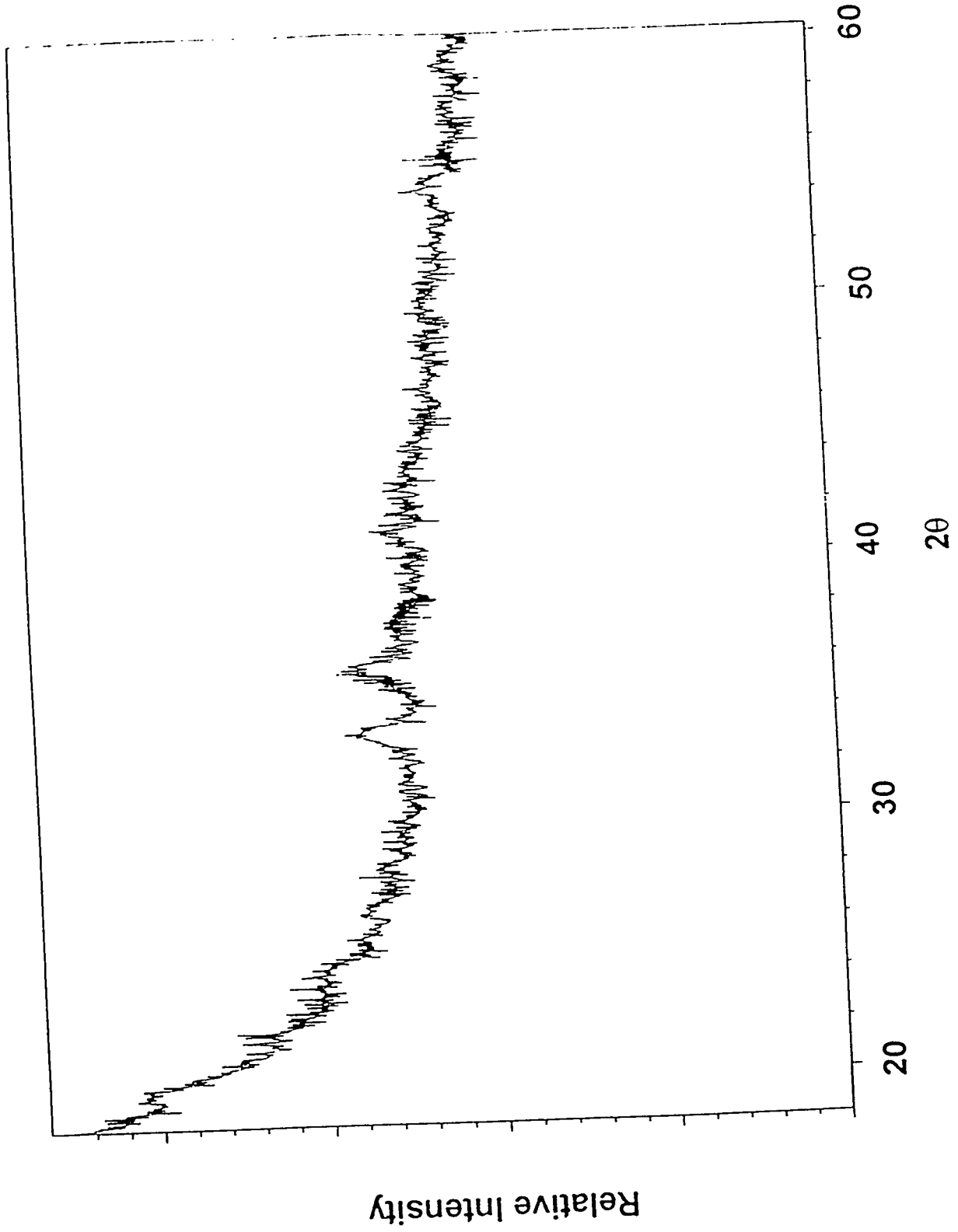


Figure 4 XRD of the delaminated/pillared clay. The broad and weak peaks at  $33.43^\circ$  and  $35.79^\circ$  are reflections of (104) and (110) faces of hematite.

Where  $L$  is the mean dimension of the crystallites,  $K$  is Scherrer constant and for spheres,  $K = 0.893 (\beta_{1/2})$ ,  $\lambda$  is the wavelength of Cu  $K\alpha$  which is 1.5418 Å,  $\beta$  is the breadth (line width at half height,  $\beta_{1/2}$ ) of the pure diffraction profile on  $2\theta$  scale in radians, and  $\theta$  is the diffraction angle.

The value of  $\beta$  was calculated by the following procedure (36): By using the breadths of silicon standard ( $b_0$ ) and catalyst sample ( $B_0$ ) from their XRD profiles and finding the  $K\alpha$  doublet separation of Cu radiation from the literature, the corrected breadths of silicon standard ( $b$ ) and catalyst sample ( $B$ ) were obtained. With the ratio of  $b/B$ , the  $\beta$  value was found from the curves for correction integral breadths of Debye-Scherrer lines for instrumental broadening. The value of  $\beta$  was found to be 0.6163. Therefore, the average  $\alpha$ - $Fe_2O_3$  particle size was 170 Å.

#### Characterization of the Delaminated PILC by Mössbauer Spectroscopy

In the case of the delaminated iron pillared clay, there are three distinct sources of iron for the spectra. First, there is the 3.8% iron in the bentonite clay, the  $Fe_2O_3$  pillars, and the larger  $Fe_2O_3$  170Å particles. Mössbauer spectrum of Wyoming bentonite has appeared in the literature (47), as well as the iron oxide pillared clay (48-50) and the larger  $Fe_2O_3$  particles on  $SiO_2$  (51-54). Ion exchanged iron is not expected due to the calcination step in the preparation of the catalyst (55).

Two spectra of the delaminated iron pillared clay were taken. The first spectrum was taken over the range  $\pm 10$  mm/sec and is shown in Figure 5. The magnetically split component was fit to a sextuplet and the superparamagnetic center component was fit to a doublet. Since the superparamagnetic components were difficult to resolve at this velocity range, the second spectrum was taken over the range of  $\pm 4$  mm/sec and is shown in Figure 6. The parameters of the sextuplet from Figure 5 were entered as invariants in the fitting procedure used to fit the spectrum in Figure 6. As is characteristic of pillared clays (47-50) and other small  $Fe_2O_3$  particles (56), the better resolved superparamagnetic component of the spectrum was fit with two doublets.

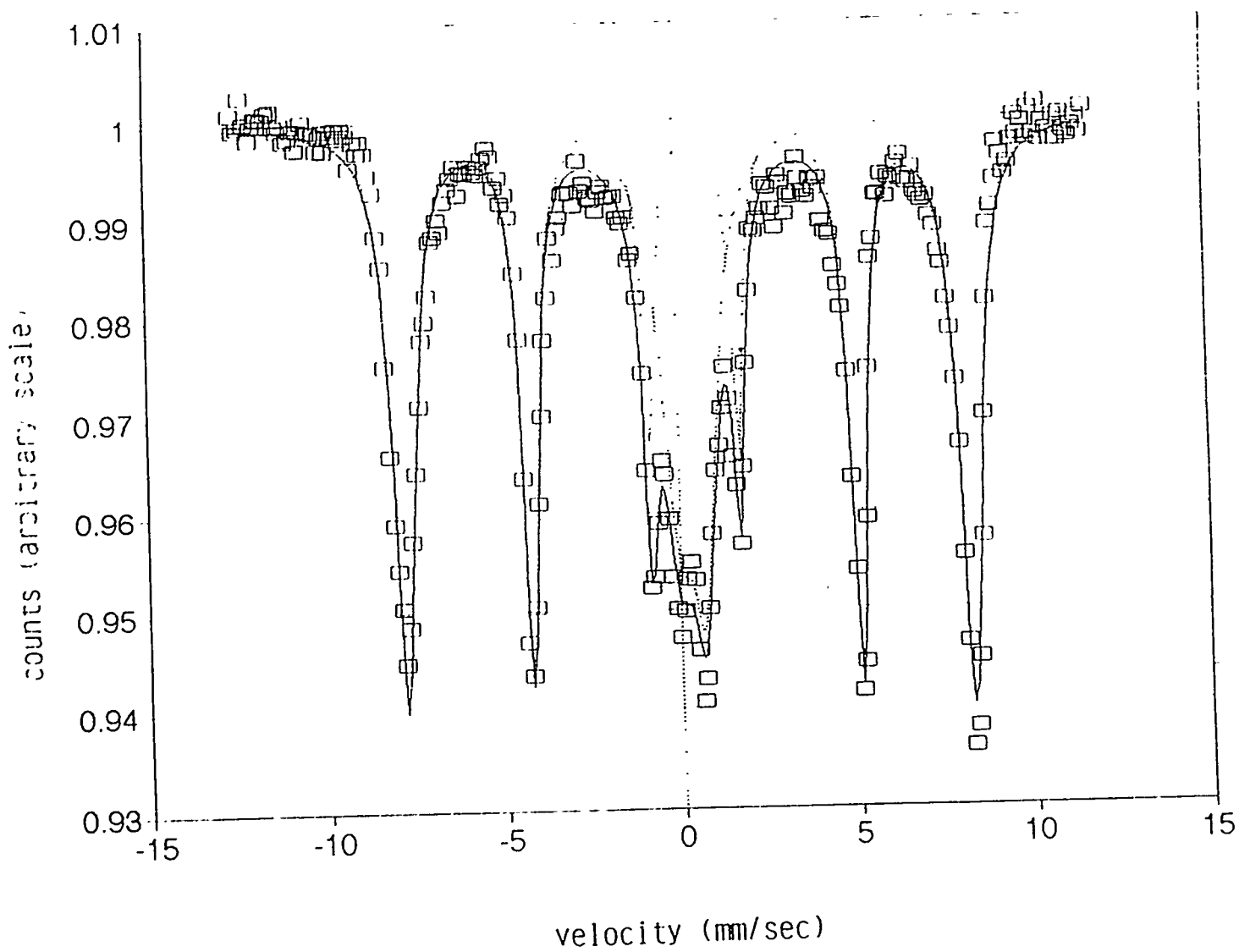


Figure 5 Mössbauer spectrum of delaminated/pillared clay in the range of  $\pm 10$  mm/sec.

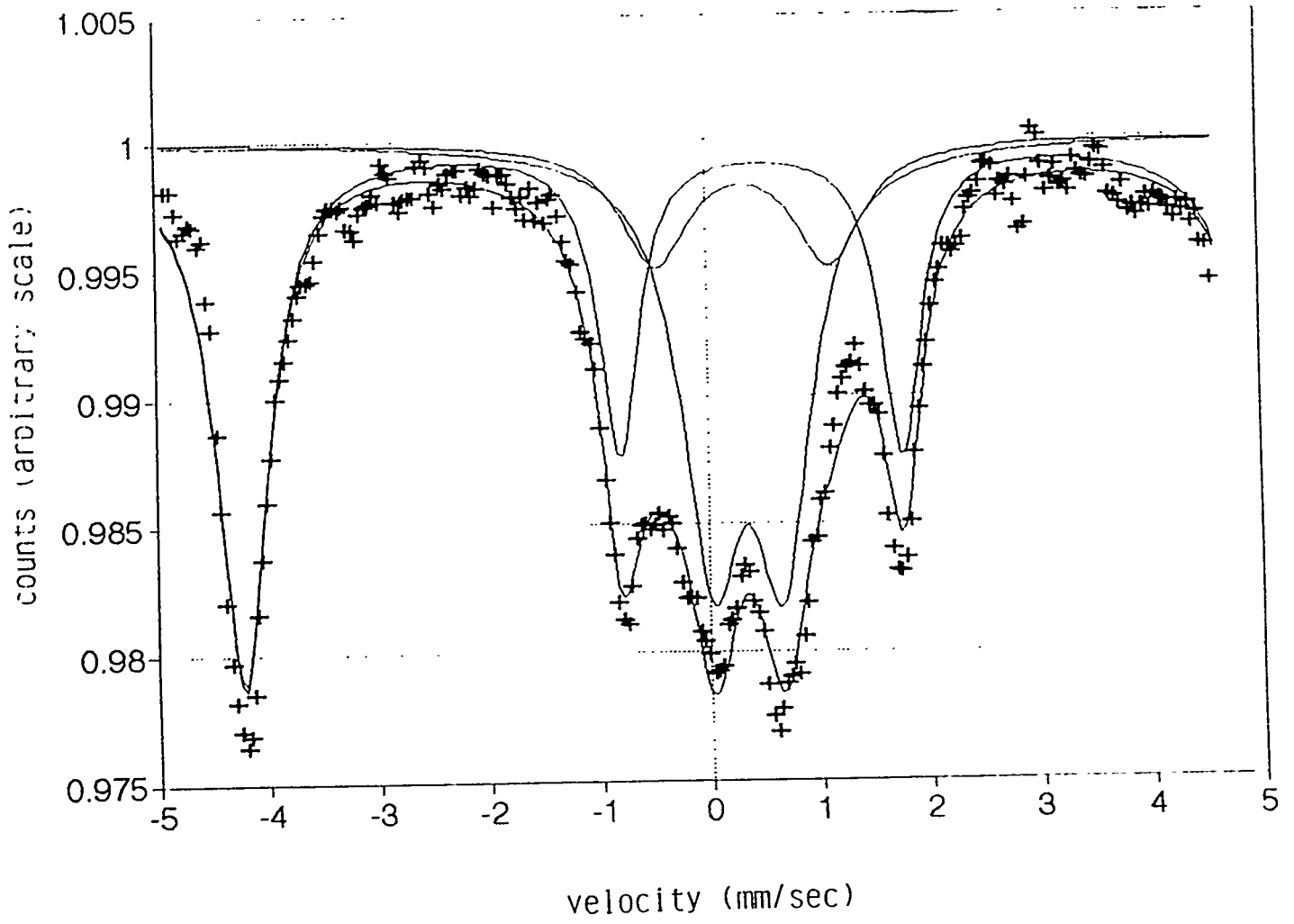


Figure 6 Mössbauer spectrum of delaminated/pillared clay with best fit (see text).

In the case of the magnetically split sextuplet, only the large 170Å particles will contribute. The hyperfine splitting was determined to be 500 kOe, which is well below the accepted 515-518 kOe value for bulk Fe<sub>2</sub>O<sub>3</sub>. The reduction in the hyperfine field is indicative of small iron oxide particles exhibiting magnetic relaxation. This is because the magnetic ordering is temperature and particle volume dependent (51-59). This particle volume dependence can be used to give an estimate of the particle size. From Table 2, it is apparent that the size of the larger Fe<sub>2</sub>O<sub>3</sub> particles can be estimated to be about 170Å, which agrees with the particle size calculations from XRD line broadening. Table 3 gives a summary of the superparamagnetic portion of the spectra reported in Table 2.

The superparamagnetic portion of the spectrum will have contributions from all three of the iron sources. The clay itself contains four different species including Fe<sup>2+</sup> and hematite (47). No attempt to include Fe<sup>2+</sup> in the fitted spectrum is made since the doublet due to the Fe<sup>2+</sup> would be difficult to quantify. The iron oxide pillars will also give a contribution to the superparamagnetic part of the spectra, as well as the superparamagnetic portion of the spectra due to the 170Å Fe<sub>2</sub>O<sub>3</sub> particles. Table 4 reports the two doublets fit from Figure 6 and compared to other literature values.

All of the iron oxide in the delaminated iron oxide pillared clay was octahedrally coordinated, since the pillars and the larger 170Å particles were bulk Fe<sub>2</sub>O<sub>3</sub> and the Fe<sup>3+</sup> in the clay itself has been shown to be octahedral (47). Thus, the isomer shift for the two doublets should be at least 0.3 mm/sec (62-64). Several "fitted" spectra of Figure 6 were discarded because the isomer shift of doublet II was too small. This is consistent with other results (47-52, 56).

It has been suggested that the outer doublet, doublet II, corresponds to the bulk or core quadrupole splitting (49,56). The surface shell has a larger quadrupole splitting due to the different electric field gradient at the surface when compared to the core. Upon examination of Table 4, one notes that there are large variations in the quadrupole splitting of doublet I. These variations could be due to different amounts of adsorbed water in the pillared clay pores (57,58).

**Table 2. The Magnetically Split Component from Figure 5 Compared to Supported Fe<sub>2</sub>O<sub>3</sub>/SiO<sub>2</sub> Literature**

<b>Hyperfine Field (kOe)</b>	<b>Isomer Shift (mm/sec)</b>	<b>Identified Species</b>	<b>Reference</b>
496	-	158 Å particles Fe <sub>2</sub> O <sub>3</sub> /SiO <sub>2</sub>	55
500	0.38	170 Å particles Fe <sub>2</sub> O <sub>3</sub> /bentonite	this work (Figure 5)
503	0.38	180 Å particles Fe <sub>2</sub> O <sub>3</sub> /SiO <sub>2</sub>	51
518	0.39	bulk Fe <sub>2</sub> O <sub>3</sub>	51

**Table 3. The Superparamagnetic Component from Figure 5 Compared to Supported Fe<sub>2</sub>O<sub>3</sub>/SiO<sub>2</sub> Literature**

Isomer Shift (mm/sec)	Quadrupole Splitting (mm/sec)	% Superpara- magnetic	Identified Species	Reference
0.6	0.68	45	158 Å particles Fe <sub>2</sub> O <sub>3</sub> /SiO <sub>2</sub>	52
0.34	0.74	29	170 Å particles Fe <sub>2</sub> O <sub>3</sub> /bentonite	This work (Figure 5)
0.38	0.44	14*	180 Å particles Fe <sub>2</sub> O <sub>3</sub> /SiO <sub>2</sub>	51
-	-	0	bulk Fe <sub>2</sub> O <sub>3</sub>	51

\*estimated from Figure 4 of reference 51.

Table 4. The Superparamagnetic Component from Figure 6 Compared to Literature

Doublet I: Isomer Shift (mm/sec)	Doublet I: Quadrupole Splitting (mm/sec)	Doublet I: % Relative Area	Doublet II: Isomer Shift (mm/sec)	Doublet II: Quadrupole Splitting (mm/sec)	Doublet II: % Relative Area	Reference
0.33	1.58	8	0.35	0.64	21	This work (Figure 6)
0.3	1.29	29	0.33	0.74	68	49
0.33	0.93	49	0.34	0.54	51	48
0.33	0.9	45	0.35	0.54	55	48
-	-	-	0.37	0.76	100	50

Upon examining Table 3, it is apparent from the isomer shift and the quadrupole splitting that the superparamagnetic doublet due to magnetic relaxation is contained within doublet II. In addition, Mössbauer spectra of aluminum chlorohydroxide pillared Wyoming bentonite (47) (IS = 0.35, QS = .64) also show that the superparamagnetic portion due to the  $\text{Fe}^{3+}$  in the clay itself will also be contained in doublet II. Thus, doublet I is a result of pillars in the clay. Typically, doublet I represents about 50 percent of the Mössbauer spectrum area for iron pillared clays (48, 49) so roughly 16 percent of the relative area in the spectrum may be due to pillars. This is also consistent with results from Kundig et. al., (51) whose work would suggest that only 10 percent of the relative area of the spectrum should be superparamagnetic due to 170 Å particles.

Summarizing the characterization results, the structure of the delaminated sample can be described as a "house of cards," and a schematic representation of the structure is shown in Figure 7.

### Activity for Selective Catalytic Reduction of NO by $\text{NH}_3$

Our earlier studies showed that  $\text{Fe}_2\text{O}_3$ -pillared clay exhibited a good activity and  $\text{SO}_2$  resistance for the NO selective catalytic reduction reaction (6). The NO SCR activities for the delaminated  $\text{Fe}_2\text{O}_3$ -pillared clay were measured under conditions both with and without  $\text{SO}_2/\text{H}_2\text{O}$ . The results are shown in Figs. 8 and 9. Three other high-activity catalysts were also included for comparison:  $\text{V}_2\text{O}_5 + \text{WO}_3/\text{TiO}_2$ ,  $\text{Fe}_2\text{O}_3/\text{Al}_2\text{O}_3$  and  $\text{Fe}_2\text{O}_3/\text{TiO}_2$ . The delaminated pillared clay showed higher activities over the other catalysts under conditions without  $\text{SO}_2/\text{H}_2\text{O}$ .

The  $\text{V}_2\text{O}_5 + \text{WO}_3/\text{TiO}_2$  contained 8.2%  $\text{WO}_3$  and 4.8%  $\text{V}_2\text{O}_5$ . This is a catalyst being commercially used (65,66). Under reaction conditions without  $\text{SO}_2$  and  $\text{H}_2\text{O}$ , as shown in Fig. 8, the delaminated  $\text{Fe}_2\text{O}_3$ -PILC showed the highest activities at all temperatures. Under conditions with both  $\text{SO}_2$  and  $\text{H}_2\text{O}$ , however, the delaminated  $\text{Fe}_2\text{O}_3$ -PILC exhibited inhibition effects, as shown in Fig. 9. The  $\text{SO}_2/\text{H}_2\text{O}$  inhibition was reversible, i.e. the activity recovered upon termination of  $\text{H}_2\text{O}/\text{SO}_2$ , as shown in Table 5. Also, the inhibition effect decreased with increasing temperature as shown in Fig. 9.

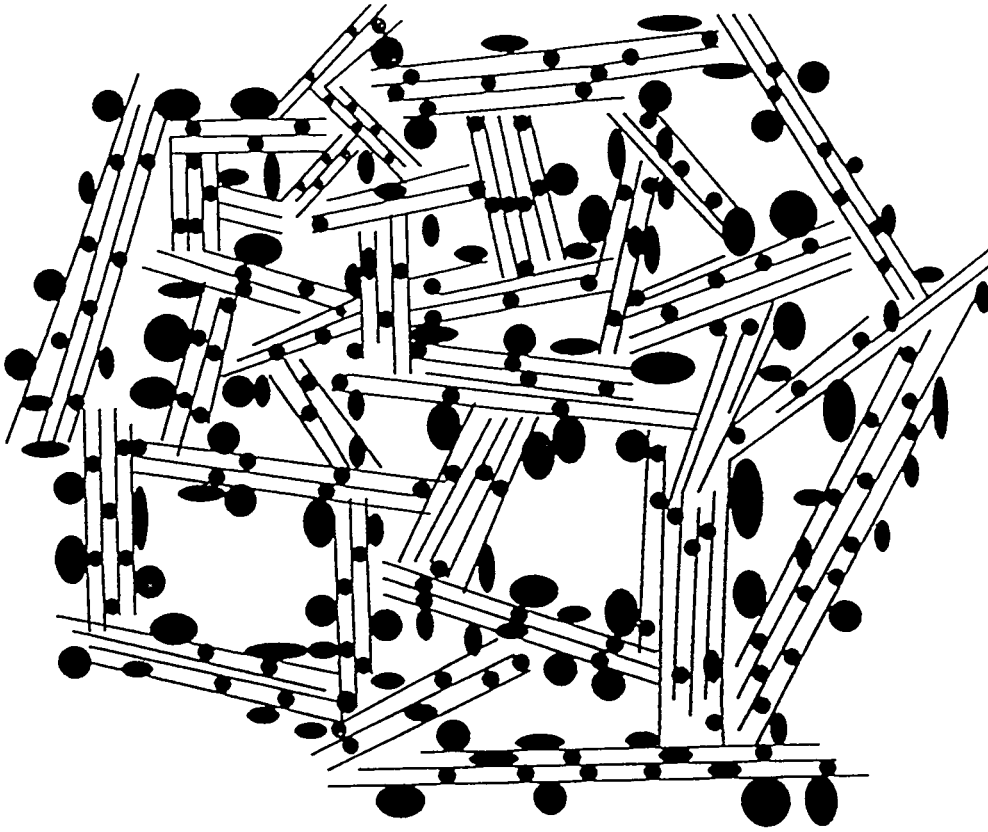


Figure 7 Schematic representation of the delaminated/pillared clay containing iron oxide particles.

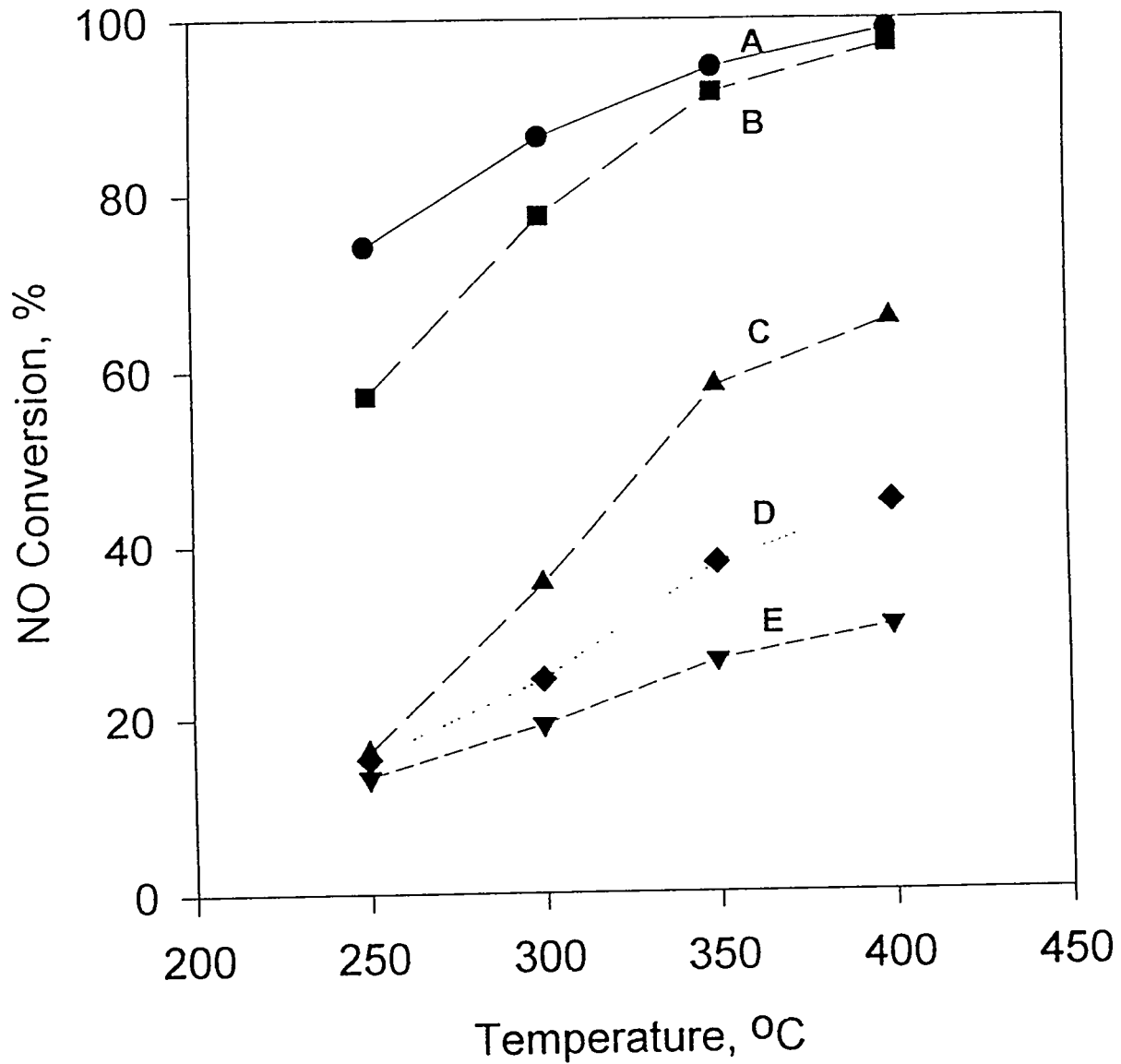


Figure 8 Selective catalytic reduction of NO with NH<sub>3</sub> on different catalysts. Reaction conditions: NO = NH<sub>3</sub> = 1,000 ppm, O<sub>2</sub> = 2%, N<sub>2</sub> balance, total flow rate = 500 ml/min., catalyst weight = 0.4 gram. A: delaminated pillared clay, B: V<sub>2</sub>O<sub>5</sub> + WO<sub>3</sub>/TiO<sub>2</sub>, C: Fe<sub>2</sub>O<sub>3</sub>-pillared clay, D: Fe<sub>2</sub>O<sub>3</sub>/Al<sub>2</sub>O<sub>3</sub> and E: Fe<sub>2</sub>O<sub>3</sub>/TiO<sub>2</sub>.

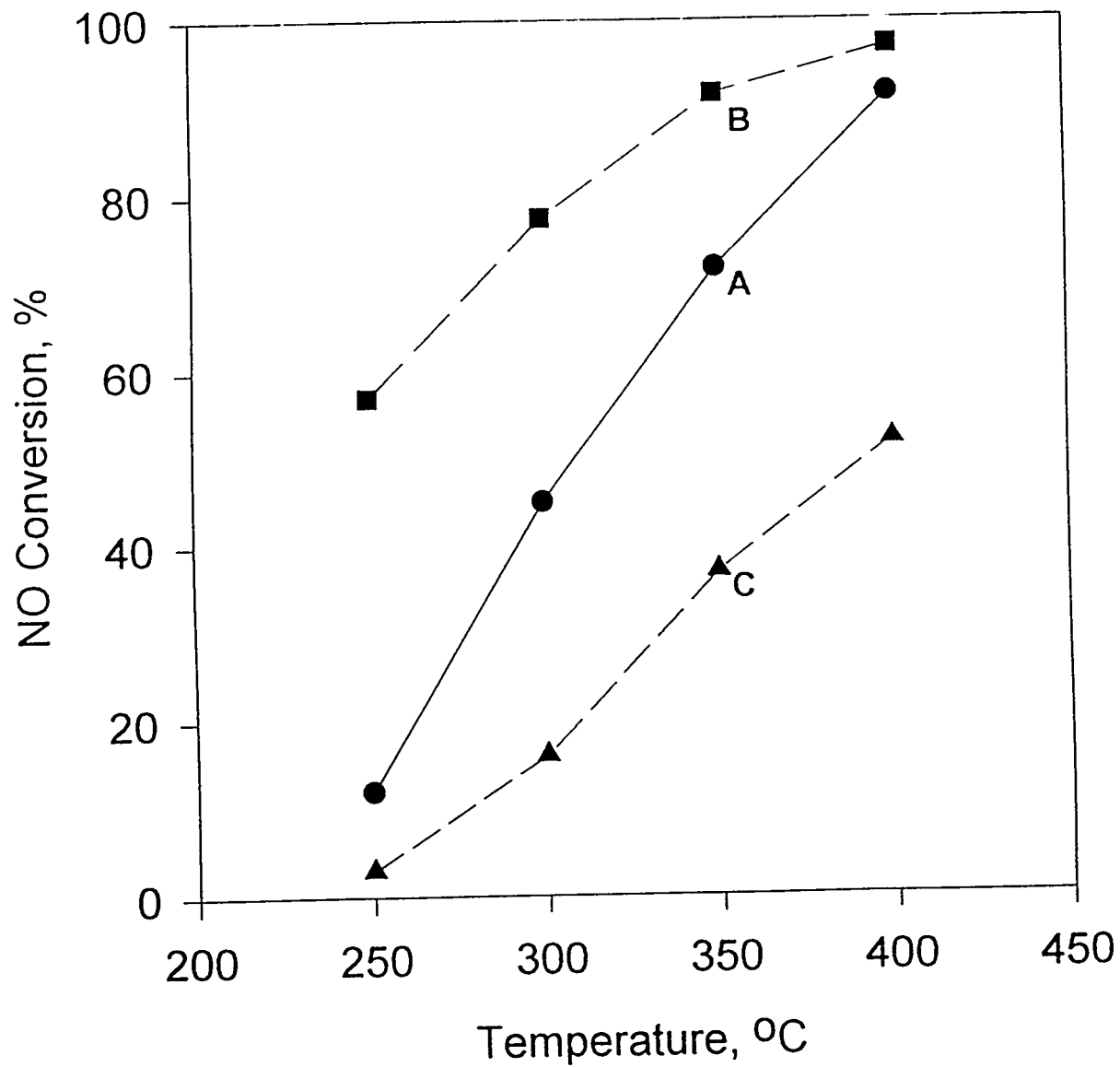


Figure 9 Selective catalytic reduction of NO with NH<sub>3</sub> on different catalysts. Reaction conditions are the same as in Fig. 8 except H<sub>2</sub>O (8%) and SO<sub>2</sub> (500 ppm) are added. A: delaminated pillared clay, B: V<sub>2</sub>O<sub>5</sub> + WO<sub>3</sub>/TiO<sub>2</sub> and C: Fe<sub>2</sub>O<sub>3</sub>-pillared clay.

From the conversion data and the reaction conditions, one may calculate the rate constants. For a plug-flow integral reactor, for first-order (with respect to NO) reaction (which was the case), and under diffusion resistance free condition (which was nearly the case in our reaction system, Chen and Yang, 1991), the rate constant (k) is given by:

$$k = -\frac{F_0}{[\text{NO}]_0 W} \ln(1 - X)$$

where  $F_0$  is the molar NO feed rate,  $[\text{NO}]_0$  is the molar NO concentration at the inlet (at the reaction temperature),  $W$  is the catalyst amount and  $X$  is the fractional NO conversion. The catalyst amount ( $W$ ) is expressed in g rather than surface area or active sites, since the true surface area (which is not the BET  $\text{N}_2$  area for microporous materials) or active sites are not known for our catalysts and no surface area information was given for the supported  $\text{Fe}_2\text{O}_3$  catalysts. From Fig. 8, the values of  $k$  (in  $\text{cm}^3/\text{g}/\text{s}$ ) are (for catalysts A to E):

At 350°C: 137(A), 125(B), 40(C), 22(D) and 15(E).

At 400°C: 176(A), 161(B), 53(C), 30(D) and 18(E).

Supported  $\text{Fe}_2\text{O}_3$  catalysts were among the most active catalysts for the NO SCR reaction (67). The data by Wong and Nobe were also included for comparison, Fig. 8, and the rate constants are given above as catalysts D and E. Wong and Nobe only studied the reaction without  $\text{SO}_2$  and  $\text{H}_2\text{O}$ , and their reactant gas composition was the same as that used in this study. Their catalyst amount was 14g and the gas flowrate was 300 liter NTP/h. So a conversion, based on first-order reaction (67) and plug flow reactor, was needed for our comparison. The conversions shown in Fig. 8 were with this conversion by using the equation above. It is seen that the two supported  $\text{Fe}_2\text{O}_3$  catalysts show lower activities than  $\text{Fe}_2\text{O}_3$ -pillared clay, as well as the other catalysts. It was further noted by Wong and Nobe that there was pore diffusion limitation in their reactions, and effectiveness factors ranging from 16% to 95% were indicated. By including the effectiveness factors, however, the NO conversion for the delaminated pillared clay was still higher than the supported  $\text{Fe}_2\text{O}_3$  catalysts.

The stability of iron oxide pillared clays have been studied by a number of researchers. It was reported that sulphite-pillared clay was stable at elevated temperatures and pressures and iron oxide pillared clay was stable under reducing conditions even at a temperature as high as 500°C (68). However, unstable iron oxide pillared clays have also been observed. SEM/EDS (Scanning Electron Microscopy/Energy Dispersive Spectroscopy) analysis (25) showed that the iron oxide pillars migrated to the edge of the clay when the pillared clay was exposed to air at ambient temperature for three months. Prompted by these reports, the delaminated pillared clay was subjected to a longevity test under the SCR conditions. As shown in Table 5, the NO conversion stayed in the range 83-86% when SO<sub>2</sub> and H<sub>2</sub>O were switched on, and the conversion was stable at 95-98% without SO<sub>2</sub> and H<sub>2</sub>O. No deactivation was shown after four days. The delaminated clay is therefore stable under the SCR reaction conditions.

### FT-IR Characterization

To examine the surface acidity and to identify the Brønsted and Lewis acid sites of the delaminated/pillared clay, FT-IR spectra of adsorbed ammonia were measured. The spectra of adsorbed ammonia at room temperature are shown in Fig. 10.

Figure 10 shows the effects of water vapor on the absorption bands at 1636.7, 1458 and 1595.1 cm<sup>-1</sup>. The peak at 1636.7 cm<sup>-1</sup> is attributed to the bending vibration of surface hydroxyl groups (69). All spectra were taken in the transmission mode, and were obtained as the ratios of the spectra after adsorption against the spectra before adsorption. In the background spectrum, a strong absorption band for the surface hydroxyl at 1636.7 cm<sup>-1</sup> appeared (not shown in Fig. 10). When NH<sub>3</sub> was introduced, it interacted with the surface hydroxyl groups forming NH<sub>4</sub><sup>+</sup>, which resulted in the strong band at 1456.9 cm<sup>-1</sup>. Therefore the negative absorption band in spectra (a) and (b) were due to the consumption of surface hydroxyl groups by ammonia adsorption, since all spectra were ratioed against that of the sample before NH<sub>3</sub> exposure. Similar negative peaks were also observed when ammonia was adsorbed on V<sub>2</sub>O<sub>5</sub>/SiO<sub>2</sub> (2). The strong peak at 1458 cm<sup>-1</sup> was due to ammonia adsorbed on Brønsted acid sites (70). The weak peak at 1595.1 cm<sup>-1</sup>

**Table 5. Longevity Test of SCR Activity for the Delaminated Fe<sub>2</sub>O<sub>3</sub> Pillared Clay**

<b>Time (hr)</b>	<b>2*</b>	<b>3</b>	<b>24</b>	<b>48</b>	<b>96</b>	<b>97*</b>
<b>NO Conversion (%)</b>	97.5	84.0	83.0	85.0	84.5	98.8

Reaction conditions: NO = NH<sub>3</sub> = 1,000 ppm, O<sub>2</sub> = 2%, SO<sub>2</sub> = 1,000 ppm (when used), H<sub>2</sub>O = 8% (when used), total flowrate = 500 ml/min, catalyst = 0.4 g, 400°C.

\*Reaction without water vapor and SO<sub>2</sub>.

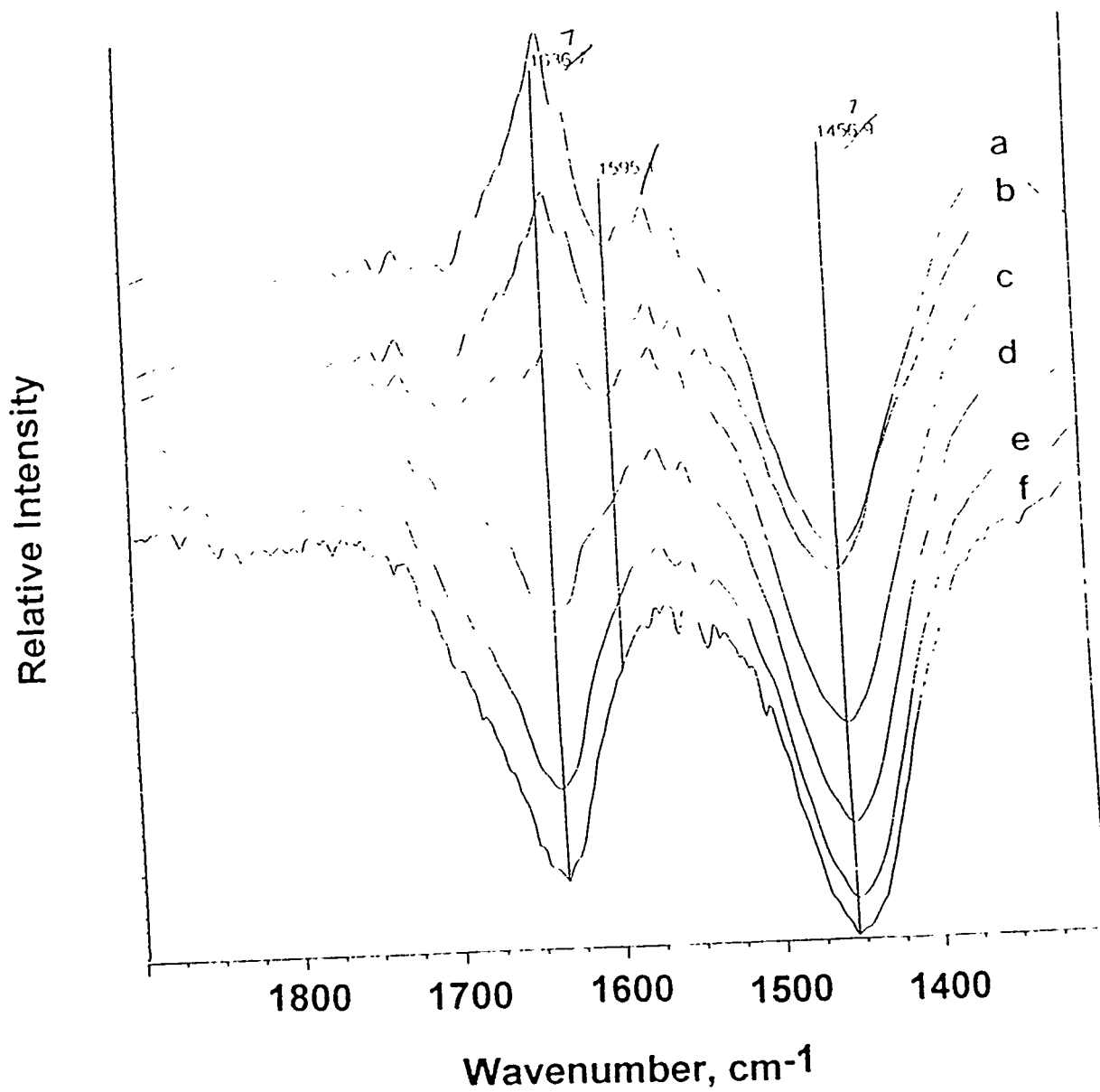


Figure 10 FT-IR spectra (transmittance) of ammonia adsorbed on delaminated  $\text{Fe}_2\text{O}_3$  pillared clay (a). (b)-(f) are after exposure to 2%  $\text{H}_2\text{O}$ , at one-minute successive time intervals. All spectra are taken at room temperature, and ratioed against the spectrum before  $\text{NH}_3$  exposure (but after calcination).

was likely due to ammonia coordinatively adsorbed on the catalyst surface, i.e., on Lewis acid sites.

Figure 10 shows that the IR band at  $1637\text{ cm}^{-1}$  changed from a negative one to a positive one, after about 3 minutes of exposure to 2%  $\text{H}_2\text{O}$ . It is interesting to note that the peak intensity at  $1458\text{ cm}^{-1}$  actually increased in the first few minutes upon  $\text{H}_2\text{O}$  exposure. Concurrently, the weak band at  $1595\text{ cm}^{-1}$  gradually decreased and eventually disappeared. This suggests that, with the addition of water vapor, the Lewis acid sites were converted to Brønsted acid sites and the coordinatively adsorbed ammonia was transformed into ammonium ions on the surface.

For clays and their variants, the surface acidity and the type of acid sites (Brønsted or Lewis sites) are dependent on the extent of hydration-dehydration. The FT-IR spectrum of ammonia adsorbed on the delaminated/pillared clay at  $150^\circ\text{C}$  is shown in Fig. 11. A very strong and sharp peak at  $1453\text{ cm}^{-1}$  was observed. The difference with the spectra taken at room temperature was that there was no negative band at around  $1630\text{ cm}^{-1}$ . This was due to dehydration at  $150^\circ\text{C}$  which eliminated the adsorbed water molecules.

The I.R. results showed that the delaminated/pillared clay was abundant in Brønsted acid sites on the surface. As shown in our previous work (4,65,71,72) Brønsted acid sites on  $\text{V}_2\text{O}_5$  and other oxides are the active sites for selective catalytic reduction of  $\text{NH}_3$  with  $\text{NO}$ . The high catalytic activity for SCR of this clay catalyst may be correlated with its strong Brønsted acidity.

Figure 12 shows the IR spectra of ammonia adsorbed on montmorillonite and the delaminated/pillared clay on the same intensity scale. Ammonia adsorbed on montmorillonite also gave an absorption band at around  $1450\text{ cm}^{-1}$ , but its relative intensity was low. It is known that there are only Lewis acid sites on  $\text{Fe}_2\text{O}_3$  (73,74). The origin of the strong Brønsted acid sites in this clay catalyst was probably the result of the interactions between  $\text{Fe}_2\text{O}_3$  and the clay. Further studies of these interactions are in progress.

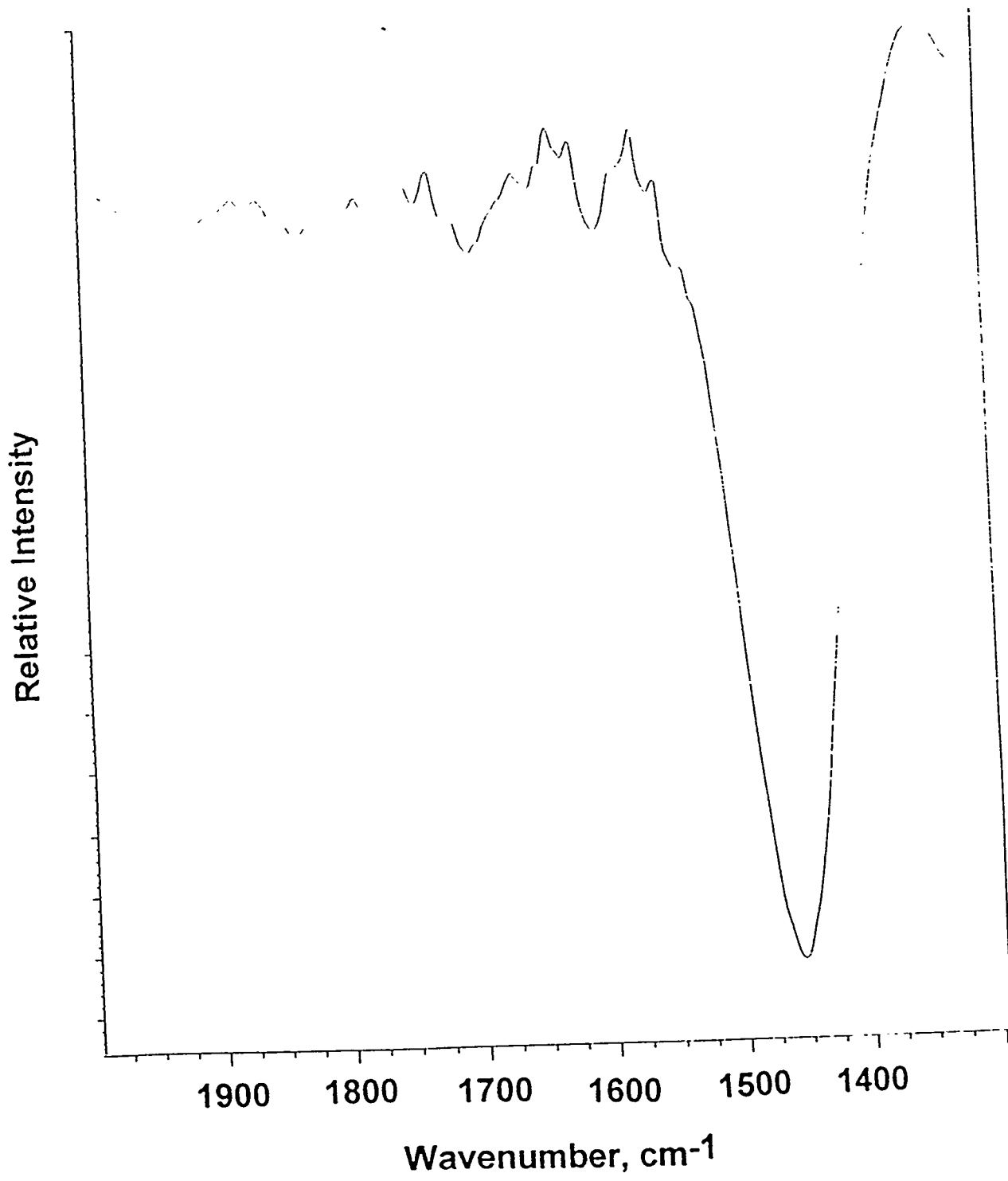


Figure 11 FT-IR spectra (transmittance) of ammonia adsorbed on delaminated/pillared clay at 150°C.

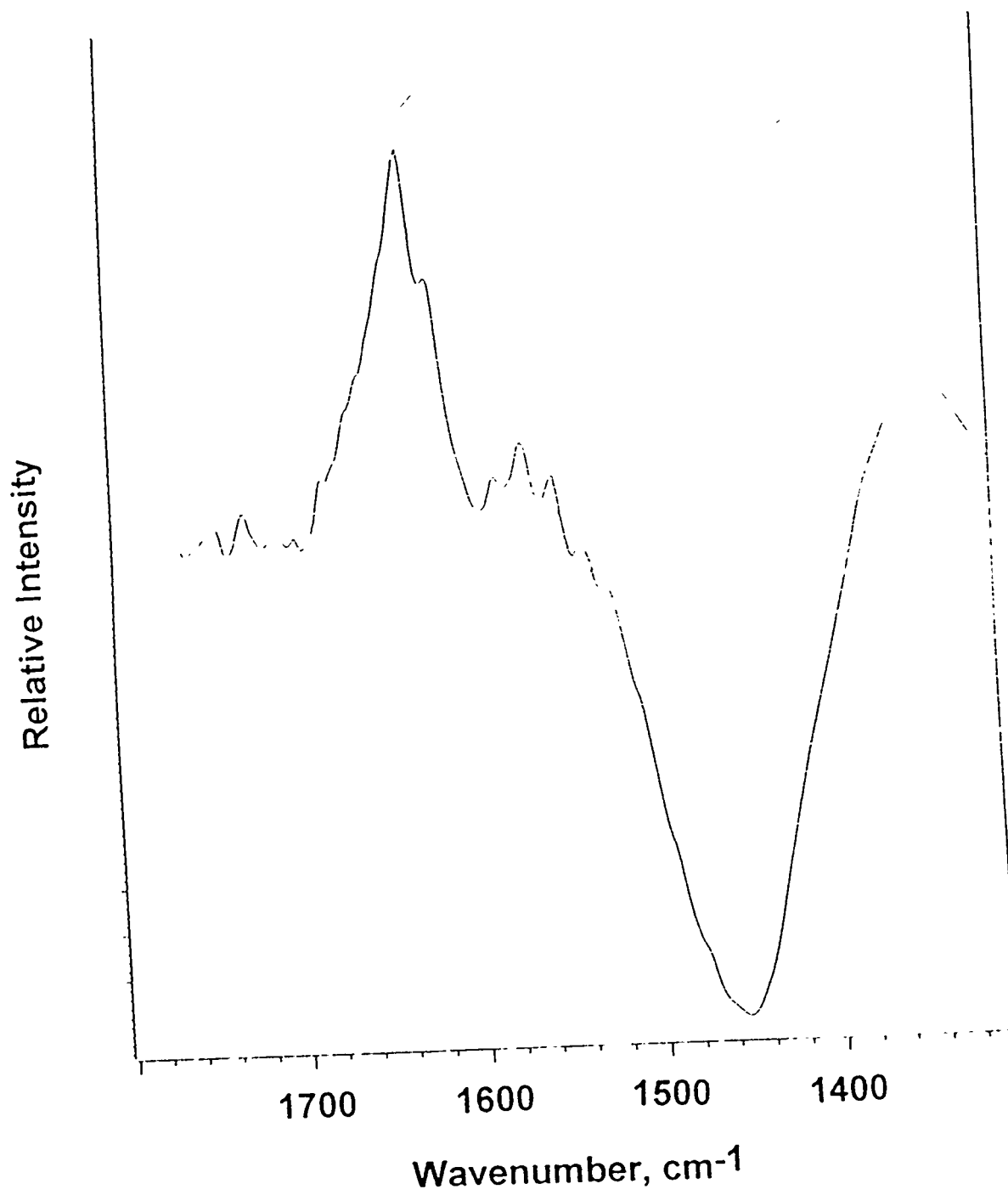


Figure 12 FT-IR spectra (transmittance) of ammonia adsorbed on montmorillonite (top) and ammonia adsorbed on delaminated/pillared clay (bottom) at room temperature.

**REFERENCES**

1. Bosch, H., and Jassen, F., Catal. Today, **2**, 369 (1988).
2. Rajadhyaksha, R.A., and Knözinger, H., Appl. Catal., **51**, 81 (1989).
3. Rajadhyaksha, R.A., Hausinger, G., Zeilinger, H., Ramstetter, A., Schmelz, H., and Knözinger, H., Appl. Catal., **51**, 67 (1989).
4. Chen, J.P. and Yang, R.T., J. Catal., **125**, 411 (1990).
5. Topsoe, N.Y., J. Catal., **128**, 499 (1991).
6. Yang, R.T., Chen, J.P., Kikkinides, E.S., Cheng, L.S., and Cichanowicz, J.E., Ind. Eng. Chem. Res., **31**, 1440 (1992).
7. Brindley, G.M. and Sempels, R.E., Clays Clay Minerals, **12**, 229 (1977).
8. Vaughan, D.E.W., Lussier, R.J. and Magee, J.S., Pillared Interlayered Clay Materials Useful as Catalyst and Sorbents. U.S. Patent 4,176,090, 1979.
9. Lahav, N., Shani, N. and Shabtai, J., Clays Clay Miner., **26**, 107 (1978).
10. Loeppert, R.H., Mortland, M.M. and Pinnavaia, T.J., Clays Clay Miner., **27**, 201 (1979).
11. Occelli, M.L. and Tindwa, R.M., Clays Clay Miner., **31**, 22 (1983).
12. Pinnavaia, T.J., Science, **220**, 365 (1983).
13. Burch, R., Catal. Today, **2**, 185 (1988).
14. Figueras, F., Catal. Rev. Sci. Eng., **30**, 457 (1988).
15. Baes, C.F., and Mesmer, R.E., The Hydrolysis of Cations, Wiley, New York, 1976.
16. Clearfield, A., NATO ASI Ser., Ser. C, **231**, 271 (1988).
17. Drezdon, M.A., Inorg. Chem., **27**, 4628 (1988).
18. Sprung, R. Davis, M.E., Kauffman, J.S. and Dybowski, C., Ind. Eng. Chem. Res., **29**, 213 (1990).
19. Occelli, M.L., Landau, S.D., and Pannavaia, T.J., J. Catal., **90**, 256 (1984).
20. Yang, R.T., and Baksh, M.S.A., AIChE J., **37**, 679 (1991).
21. Baksh, M.S.A., Kikkinides, E.S., and Yang, R.T., Ind. Eng. Chem. Res., **31**, 2182 (1992).
22. Burch, R. and Warburton, C.I., J. Catal., **97**, 511 (1986).

23. Occelli, M.L., Innes, R.A., Hwu, F.S.S. and Hightower, J.W., Appl. Catal., 14, 69 (1985).
24. Occelli, M.L., Hsu, J.T. and Galya, L.G., J. Mol. Catal., 33, 371 (1985).
25. Rightor, E.G., Tzou, M.S. and Pinnavaia, T.J., J. Catal., 130, 29 (1991).
26. Czarnecki, L.J. and Anthony, R.G., AIChE J., 36, 794 (1990).
27. He, M.Y., Liu, Z. and Min, E., Catal. Today, 2, 321 (1988).
28. Jones, W., Catal. Today, 2, 357 (1988).
29. Tennakoon, D.T., Jones, W., Thomas, J.M., J. Chem. Soc. Faraday Trans. I., 82, 3081 (1986).
30. Molinard, A., Peeters, K.K., Maes, N. and Vansant, E.F., "Separation Technology," Ed. by E.F. Vansant, Elsevier, New York, p. 445 (1994).
31. Beeckman, J.W. and Hegedus, L.L., Ind. Eng. Chem. Res., 30, 969 (1991).
32. Pinnavaia, T.J., Tzou, M-S., Landau, S.D., Raythatha, R., J. Mol. Catal., 27, 195 (1984).
33. Occelli, M.L., Landau, S.D., Pinnavaia, T.J., J. Catal., 104, 331 (1987).
34. Pinnavaia, T.J., Tzou, M.S., Landau, S.D., and Raythatha, R.H., J. Mol. Catal., 27, 195 (1984).
35. Occelli, M.L., Catal. Today, 2, 339 (1988).
36. Klug, H.P., and Alexander, L.E., "X-Ray Diffraction Procedures -- For Polycrystalline and Amorphorous," 2nd Ed., Wiley, New York, Chapt. 9, (1974).
37. Newman, A.C.D., and Brown, G., "The Chemical Constitution of Clays," in "Chemistry of Clay and Clay Minerals," Wiley, New York, 1987: and the literature cited therein.
38. Klug, H.P., and Alexander, L.E., "X-Ray Diffraction Procedures -- For Polycrystalline and Amorphorous," 2nd Ed., Wiley, New York, p. 667 (1974).
39. Bailey, S.W., "Structures of Clay Minerals and Their X-Ray Identification," Ed by Brindley, G.W. and Brown, G., Mineralogical Society Monograph, No. 5, Mineralogical Society, London, 1980.
40. Reference (39), P. 171.

41. Mott, C.J.B., "Clay Minerals - An Introduction," in "Pillared Clays," Ed by Burch, R., Catalysis Today, 2, 187 (1988).
42. Burch, R., and Warburton, C.I., J. Chem. Soc., Chem. Commun., 117 (1987).
43. Pinnavaia, T.J., Tzou, M.S., and Landau, S.D., Pillared and Delaminated Clays Containing Chromium, U.S. Patent, 4,665,045, May 12, 1987.
44. Occelli, M.L., Landau, S.D., Pinnavaia, T.J., J. Catal., 104, 331 (1987).
45. Gregg, S.J. and Sing, K.S.W., "Adsorption, Surface Area and Porosity," Academic Press, London, 2nd Ed., 1982.
46. Reference (38), p. 371 and the literature cited therein.
47. Occelli, M.L., Stencel, J.M., Suib, S.L., J. Mol. Catal., 64, 221 (1991).
48. Martin-Luengo, M.A., Martins-Carvalho, H., Ladriere, J., Grange, P., Clay Minerals, 24, 505 (1989).
49. Doff, D.H., Gangas, N.H.J., Allan, J.E.M., Coey, J.M.D., Clay Minerals, 23, 367 (1988).
50. Lee, W.Y., Raythatha, R.H., Tatarchuk, B.J., J. Catal., 115, 159, (1989).
51. Kundig, W., Bömmel, H., Constabaris, G., Lindquist, R.H., Phys. Rev., 147 No. 2, 327 (1966).
52. Hobson, M.C., Gager, H.M., J. of Catal., 16, 254 (1970).
53. Yoshioka, T., Koezuka, J., Ikoma, H., J. Catal., 16, 264 (1970).
54. Lund, C.R.F., Dumesic, J.A., J. Phys. Chem., 85, 317 (1981).
55. Helson, J.A., Goodman, B.A., Clays Minerals, 18, 117 (1983).
56. Kundig, W., Ando, K.J., Lindquist, R.H., Constabaris, G., Czech. J. Phys., B17, 467 (1967).
57. Topsoe, H., Boudart, M., J. Catal., 31, 346 (1973).
58. Mørup, S., Topsoe, H., Appl. Phys., 11, 63 (1976).
59. Mørup, S., Dumesic, J.A., and Tøpsoe, H., "Applications of Mossbauer Spectroscopy," (R. Cohen, Ed.), Vol. Academic Press, New York, 1980.
60. Gager, H.M., Hobson, M.C., Lefelhocz, J.F., Chem. Phys. Lett., 15 no.1, 124 (1972).
61. Gager, H.M., Lefelhocz, J.F., Hobson, M.C., Chem. Phys. Lett., 23 no.3, 386 (1973).

62. Meagher, A., Zeolites, 9, 87, (1989).
63. Garten, R.L., Delgass, W.N., Boudart, M., J. Catal., 18, 90 (1970).
64. Coey, J.M.D., Atomic Energy Review, 18 no. 1, 73 (1980).
65. Chen, J.P., and Yang, R.T., Appl. Catal., 80, 135 (1992).
66. Tuenter, G., Leeuwen, W.F.V., and Snepvangers, L.J.M., Ind. Eng. Chem. Prod. Res. Dev., 25, 633 (1986).
67. Wong, W.C. and Nobe, K., Ind. Eng. Chem. Prod. Res. Dev., 25, 179 (1986).
68. Thomas, J.M., and Theocharis, C.R., "Catalysis with Clays and Their Pillared Variants," in "Perspectives in Catalysis - Chemistry for the 21st Century," p. 478, Blackwell Scientific Publications, Oxford, 1992.
69. Little, L.H., "Infrared Spectra of Adsorbed Species," Academic Press, London, 1966.
70. Kung, M.C. and Kung, H.H., Catal. Rev.-Sci. Eng., 27, 425 (1985).
71. Chen, J.P., and R.T. Yang, J. Catal., 139, 277 (1993).
72. Chen, J.P., Yang, R.T., Buzanowski, M.A., and Cichanowicz, J.E., Ind. Eng. Chem. Res., 29, 1431 (1990).
73. Rochester, C.H., and Topham, S.A., J. Chem. Soc., Faraday Trans. I, 75, 1259 (1979).
74. Peri, J.B., J. Phys. Chem., 69, 220 (1965).
75. Warburton, C.I., in "Pillared Clay," (Ed. R. Burch), Catal. Today, 2, 275 (1988).